sustainability

MDPI

Article

Variations in Permeability and Mechanical Properties of Basaltic Rocks Induced by Carbon Mineralization

Zhenni Ye [1,2,*], Xiaoli Liu [3,*], Huan Sun [1,2], Qinxi Dong [1,2], Weisheng Du [4] and Qijian Long [1]

[1] School of Civil Engineering and Architecture, Hainan University, Haikou 570228, China
[2] Collaborative Innovation Center of Ecological Civilization, Hainan University, Haikou 570228, China
[3] State Key Laboratory of Hydroscience and Engineering, Tsinghua University, Beijing 100084, China
[4] Deep Mining and Rock Burst Research Branch, Chinese Institute of Coal Science, Beijing 100013, China
* Correspondence: zn.ye@hainanu.edu.cn (Z.Y.); xiaoli.liu@mail.tsinghua.edu.cn (X.L.)

Abstract: Carbon capture, utilization, and storage (CCUS/CCS) is a strategic choice for ensuring energy security and reducing carbon dioxide emissions across the globe. The injection of CO_2 into the basaltic reservoir is one strategy for the permanent disposal of carbon emissions. Basaltic rocks, which are widely distributed in Hainan Island, are capable of CO_2 geological sequestration. In this study, the reaction of CO_2-NaOH/$Ca(OH)_2$-basaltic rocks under conditions of 6.0 M Pa and 30 °C was performed using basaltic samples collected from the Fushan area of the Hainan Province to evaluate the sequestration of CO_2 in basalt by mineralization. Then, the effect of CO_2 mineralization on the permeability and mechanical properties of basaltic rocks was evaluated using X-ray computer tomography and triaxial compression testing at 21.0 MPa. In addition, microwave technology was used to irradiate the basaltic rocks before mineralization. Changes in the permeability of basalt before and after mineralization and microwave irradiation were simulated numerically, and their effects on the mechanical strength deterioration of basalt were analyzed according to the rock mechanics using triaxial testing. Based on these results, a new method for the induction of basalt deterioration, mineralization, CO_2 injectivity, and storage capacity using microwave irradiation is proposed for use in CCUS/CCS engineering.

Keywords: basaltic rocks; absolute permeability; rock strength; carbon mineralization; microwave irradiation

Citation: Ye, Z.; Liu, X.; Sun, H.; Dong, Q.; Du, W.; Long, Q. Variations in Permeability and Mechanical Properties of Basaltic Rocks Induced by Carbon Mineralization. *Sustainability* **2022**, *14*, 15195. https://doi.org/10.3390/su142215195

Academic Editor: Jianjun Ma

Received: 13 October 2022
Accepted: 14 November 2022
Published: 16 November 2022

1. Introduction

The Chinese government recently included the objectives of "Emission Peak" and "Carbon Neutrality" into their overall planning for the establishment of an ecological and sustainable society. The development of technology for use in carbon dioxide capture, utilization, and storage (CCUS/CCS) is a strategic choice aimed at reducing carbon dioxide emissions and ensuring energy security in the future. In China, Hainan Province has been chosen by the government as the national low-carbon pilot province, wherein the government is promoting the construction of a free-trade port. This province is comprised of 35,400 km^2 of land and 2 million km^2 of sea under the jurisdiction of the local authorities. Within the province, there are oil and gas-bearing strata and saltwater layers in the Weizhou Formation and Liushagang Formation in the Fushan Basin, with unique CO_2 geological storage conditions and marine geological environment resources. In particular, volcanic rocks are widely found in Hainan Island, with an exposed area of about 18,000 km^2, accounting for 53% of the island's area.

Basaltic rocks are the most widely distributed rocks on the planet, covering large areas of the continents and the seafloor of oceans. Basalt is rich in calcium, magnesium, and iron, which enables mineralization and the generation of solid carbonate minerals under CO_2 injection. Since this method does not require low permeability strata, such as caprocks [1], basalt strata are ideal sites for the permanent disposal of CO_2. Recently,

Hengill geothermal power plant in southwest Iceland successfully injected CO_2 into the basalt stratum to permanently store CO_2 by mineralization.

Fushan Sag in Hainan Province is comprised of 78 layers of basalt strata, with a total thickness of 380 m. A CCUS pilot project in a Fushan oilfield injected supercritical CO_2 into oil and gas reservoirs to improve formation pressure and displace oil and gas for production. Deep saline water layers and basalt layers are potential sites for future CCS projects. Stimulating the mineralization of rocks, geofluids, and carbon dioxide to convert them into carbonate minerals minimizes the risk of CO_2 leakage and has become a popular strategy for long-term safe carbon storage. However, Hainan Province faces many practical issues due to the extensive presence of cement, petrochemical, and chemical industries, which emit CO_2. In particular, with the aim of achieving zero carbon emissions, the petrochemical industry in Yangpu specifically needs to develop and apply CCS technology. However, the feasibility of the use of CO_2 geological storage technology is highly dependent on the lithology and hydrogeological environment of regions with high carbon emission industries. In this study, to determine the conditions most favorable for CO_2 mineralization and storage in basalt in highly industrialized areas in China, high-pressure mineralization reaction experiments using basalt, liquid CO_2, and a solution NaOH and $Ca(OH)_2$ were performed in Hainan Island. As a result, the injectability and storage of CO_2 in basalt were evaluated. The reactions of basalt mineralization and basalt subjected to microwave irradiation were compared to verify the feasibility of CO_2 mineralization and storage in shallow buried depths in Hainan Island.

The previous theory and the technology of CO_2 mineralization and CO_2 storage in basalt have made considerable advances worldwide. As early as 1990, scholars proposed mineral transformation to capture and store CO_2 [2]. Silicate minerals, which are rich in calcium and magnesium, can react with CO_2 to form stable carbonate minerals. Continental overflow basalt has been demonstrated to be capable of CO_2 mineralization and sealing, with an internal porosity and lateral connectivity that enable CO_2 injection [3]. However, the internal mineral composition, pore structure, fissure structure, and water-bearing characteristics of overflow basalt tend to vary under different environmental and geological conditions [4]. The interaction between exposed basalt and atmospheric CO_2 results in a natural carbon sink. The pores on the surface of basalt associate with CO_2 in the atmosphere and naturally form carbonate particles. Calcite commonly observed on the surface of common porphyry basalt is evidence of this reaction. In addition to acting as a natural carbon sink, the ability of basalt to permanently seal CO_2 is the result of a chemical reaction between CO_2 and the rock that produces carbonate. Matter, Kelemen [5] found that when CO_2 was injected into basalt, the chemical process of mineralization included CO_2 dissolution in an aqueous solution and rock dissolution in a water-soluble solution. During this reaction, the liquid and separated divalent metal cations and the carbonate ions reacted with divalent cations and formed sediments. In another study, Kelemen, Matter [6] investigated potential factors influencing the process of CO_2 mineralization in basalt, including temperature, pressure, pH value, fluid flow rate, and other factors. As a result, they found that the CO_2 mineralization sealing efficiency depends on the dissolution rate of rock minerals and the precipitation reaction of carbonate minerals, where pH value was a significant reaction parameter. Similarly, Park, and Fan [7] found that a low pH environment is beneficial to the dissolution of silicate minerals. Seifritz, W. [2] also found that a high pH environment is more conducive to the formation and precipitation of carbonate minerals. In addition to the literature on CO_2 mineralization and sealing theory, the permeability and mechanical strength of basalt reservoirs in CCS projects are important factors that determine the injectability and engineering storage potential of CO_2. Callow et al. [8] conducted X-ray CT analysis on the core samples of a basalt reservoir in Iceland for the CarbFix project and found that the vertical permeability (2.07×10^{-10} m^2) was higher than the horizontal permeability (5.10×10^{-11} m^2). The permeability of reservoir rocks is closely related to pore diameter, as well as pore volume and connectivity [9]. Based on Kozeny Carman's model, the absolute permeability of reservoir rocks can be calculated by

measuring porosity and pore diameter [10]. Calculating the absolute permeability of basalt in the CarbFix project, Aradóttir et al. [11] found that the storage potential of Icelandic basalt formation is 100% (5,000 tons/km^2). Therefore, the characteristics and permeability of reservoir rock pores are key to evaluating carbon storage potential. However, the CO_2 capacity of long-term injectable storage is significant for CCUS or CCS projects. The mechanical strength of basalt reservoirs is closely associated with the pressure needed for CO_2 injection and reservoir cap stability. In general, the inner enriched connective pores, the larger fractures, and the lower strength of the reservoir would be more injectable for CO_2 storage. This is related to the strength of the inner structure and rocks. The published research are not involved in comparison with rock strength before and after the reaction of the CO_2 mineralization. The previous study just considered CO_2 leakage risk used pressure monitoring of injection formation and the time-delay effect as key factors [12,13]. Another important consideration of CO_2 geological storage is the stability of caprock and the risk of CO_2 escape. Interactions between water and rocks have a significant impact on rock mechanical strength [14–17]. These water-rock interactions and mineralization dissolution in CO_2 geological storage promote passive effects on rock mechanical strength. After testing fracture mechanics, Major et al. [18] concluded that water-rock interactions are beneficial in preventing fracture propagation. The propagation of subcritical fractures in mineral dissolution areas reduces the integrity of caprock [15]] and may thus impact the safety of long-term CO_2 storage.

Rock modification methods, which are currently being widely used in oil and gas production and development, coalbed methane extraction, and natural gas hydrate extraction, mainly include hydraulic fracturing [19], CO_2 acid fracturing [20], electromagnetic heating [21], and microbial transformation [22], among other methods. Microwave irradiation modification technology in underground engineering excavation has been proposed to improve the mechanical strength of extremely hard rock masses [23,24]. To study the effect of microwave irradiation on rocks, Zheng et al. [25] proposed the microwave fracturability index (MFI) of hard igneous rocks. Similarly, with the aim of studying the industrial applicability of microwave rock-breaking technology, Lu et al. [26] carried out experiments on the cracking of basalt using microwave irradiation. As a result, they found that the cracks generated by the microwave irradiation of basalt were mainly distributed between and within olivine and plagioclase particles. This was mainly due to the large amount of heat generated by enstatite and the volume expansion stress caused by olivine under microwave irradiation. However, these studies have mainly focused on the application of basalt microwave fracturing in underground projects, while research on basalt CO_2 geo-storage technology remains scarce.

If some research tasks on the injectable evaluation of the rock reservoir could be carried out in the laboratory, these experimental results would be useful guidance for CO_2 mineralization storage. In this study, the differences in the permeability and mechanical strength characteristics of basalt CO_2 before and after mineralization were evaluated to address the gap in the literature. In order to evaluate the impact of CO_2 mineralization on permeability and mechanical strength, the three-dimensional CT scanning and triaxial loading of the pore structure of basalt CO_2 before and after mineralization were performed. In addition, basalt was subjected to microwave irradiation to study the changes in the permeability and mechanical strength of basalt before and after CO_2 mineralization. In addition, the CO_2 mineralization storage effect of basalt was evaluated to determine the industrial applicability of microwave-modified storage enhancement technology. Based on these findings, a microwave-modified storage technology and a waveguide design scheme for CO_2 underground storage are proposed, providing a theoretical basis and technical guarantee for the commercialization and promotion of basalt CO_2 mineralized storage.

2. Experimental Methodology

2.1. Experiment Design and Test Scheme

In addition to the chemical action, in the CO_2 mineralization reaction of basaltic rocks, the mechanical penetration action greatly improves the speed of mineralization. In order to elucidate the mechanism of basalt CO_2 mineralization, a high-pressure reactor was used to react basalt with liquid CO_2 and an alkaline solution of NaOH and $Ca(OH)_2$. The alkaline solution was used to promote the pore and fracture space clogging in basalt. Macro- and micro-porous basaltic samples were used for the mineralization experiments.

The shallower reservoir would be more economical for carbon mineralization on the premise of adequate reaction without CO_2 leakage. Large basalt samples were collected from the basaltic samples (between the surface layer and a depth of 50.0 m, the cylindrical basalt preparation boreholes from the blocky rocks) in the Fushan Sag, Haikou City, Hainan Province, which were subsequently processed into six complete standard cylinder specimens (diameter, 50 mm; height, 100 mm). The samples of the macro-porous basalt group were denoted as B_1, B_2, and B_3, while the samples of the small-pore basalt group were denoted as S_1, S_2, and S_3, respectively. The experimental method and test flow are shown in Figure 1. For considering the CO_2 injection in situ of the Fushan CCUS project, the internal temperature of the reactor body and the actual formation temperature was approximately 30 °C, and the internal pressure of the reactor body was maintained at 6.0 MPa in the experiment. The experimental conditions are listed in Table 1. The aim of this experiment was to reveal the change in the characteristics of the microstructure and thermodynamic reaction of CO_2, basalt, and NaOH or $Ca(OH)_2$ alkaline solution before and after the mineralization. X-ray CT tomography was used to analyze the internal porosity, permeability, and other physical parameters of basalt before and after CO_2 mineralization. Finally, triaxial rock mechanics testing was used to compare the mechanical strength of basalt before and after CO_2 mineralization under 21.0 MPa of confining pressure. By focusing on the changes in the mineralization reaction degree and mechanical strength of basalt before and after microwave irradiation, this study provides data to support the further study of basalt CO_2 geological storage theory and technology application.

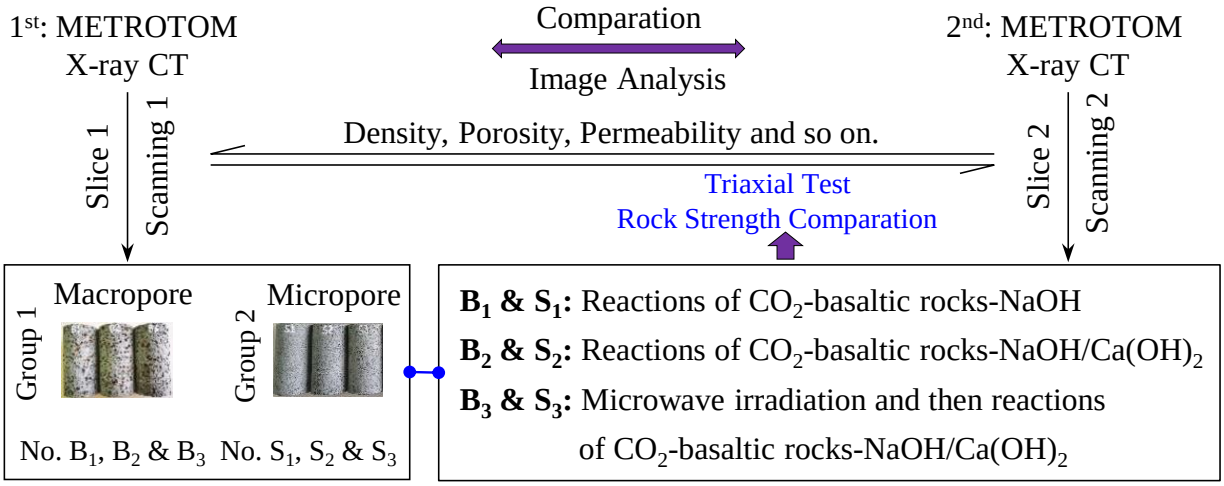

Figure 1. Experimental method for the evaluation of the pore structure and mechanical strength of basalt before and after CO_2 mineralization.

Table 1. Experimental conditions of basalt CO_2 mineralization.

Numbers	Reaction Time	NaOH Solution	$Ca(OH)_2$ Solution	Reaction Pressure/MPa	Reaction Temperature	Microwave Time
B_1	24 h	200 ml	N/A	6.0	30 °C	N/A
B_2	48 h	200 ml	200 ml	6.0	30 °C	N/A
B_3	24 h	200 ml	200 ml	6.0	30 °C	2 min
S_1	24 h	200 ml	N/A	6.0	30 °C	N/A
S_2	48 h	200 ml	200 ml	6.0	30 °C	N/A
S_3	24 h	200 ml	200 ml	6.0	30 °C	2 min

2.2. Experimental Apparatus and Rock Mechanics Testing

X-ray CT scanning technology was used to scan and reconstruct the internal structure of the basalt samples on the basis of cross-section imaging using a cone-shaped X-ray beam (Metrotom X-ray CT device). The principle of X-ray CT scanning is shown in Figure 2a. As shown in Figure 2b, X-ray CT was used to scan basalt before and after the CO_2 mineralization reaction. The voltage used directly determines the clarity of the basalt X-ray image. In this study, a voltage of 220 kV and a current of 252 μA were used. A single cylinder can obtain 2600 slice images. The X-ray images were set to DICM format for analysis.

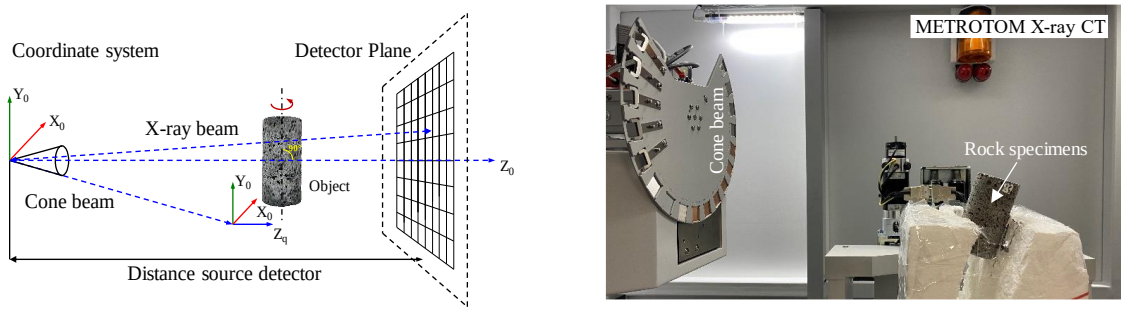

(**a**) (**b**)

Figure 2. X-ray tomography 3D scanning principle and X-ray CT equipment: (**a**) three-dimensional schematic of the design principle and (**b**) sectional schematic of the design principle.

The rock CO_2 mineralization high-pressure reactor used in this study was comprised of a steel reactor body with a CO_2 inlet interface and an internal pressure valve, as well as a pressure instrument at the interface. Through the air compressor and booster pump, the interior of the reactor could be pressurized to ensure a gradual increase in the internal reactor pressure to 6.0 MPa. The temperature control system of the reactor was used to maintain an internal temperature of 30 °C. The interior of the reactor was continuously filled with CO_2. A schematic representation of the reactor is provided in Figure 3, including the experimental principle of the basalt CO_2 mineralization reaction (Figure 3a) and the reactor device and system (Figure 3b).

The micropore structure and mechanical strength of basalt are the basis of CO_2 injectability and mineralization effect. In general, when the mechanical strength of the reservoir rock is low, the porosity is large, and the injection pressure is low, a higher amount of CO_2 injection and a better storage effect can be achieved. However, with an increase in the CO_2 injection and a deepening of the mineralization of the rock, the carbonate mineral components formed by basalt mineralization accumulate on the inner surface of the pores and fractures, resulting in the formation of dirt. Moreover, after CO_2 is injected into the reservoir rock, the pressure of the pores rises, making it difficult to dissipate the fluid pressure in the rock pores in a short time, which decreases the CO_2 injectability of basalt.

This has been demonstrated to be a good method for rock material modification to improve the internal mineral, fracture structure, and mechanical strength of reservoir rock via a thermal effect. In order to explore the effect of microwave irradiation on the internal pore fissures and mechanical strength of basalt, a microwave system with a manual three-stub tuner and a power of 6 kW and 2.45 GHz was used. In the experiment, basaltic rocks before CO_2 mineralization were irradiated for 2 min, and then the surface temperature of basalt was recorded by an infrared thermal imager. The microwave equipment and irradiation process are shown in Figure 4a, and the thermal infrared images of two types of basalt after microwave irradiation are shown in Figure 4b.

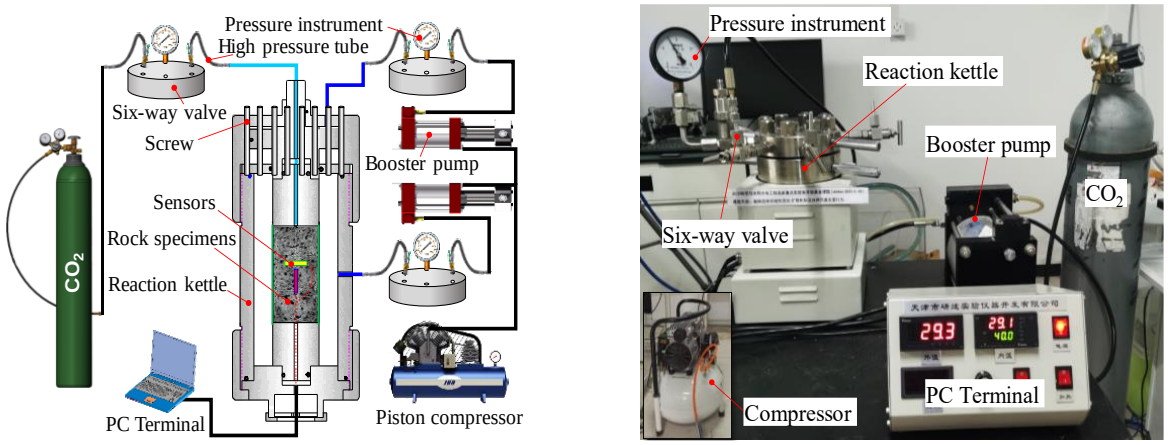

Figure 3. Experimental principle and device of basalt CO_2 mineralization: (**a**) experimental principle of basalt CO_2 mineralization and (**b**) rock reaction kettle.

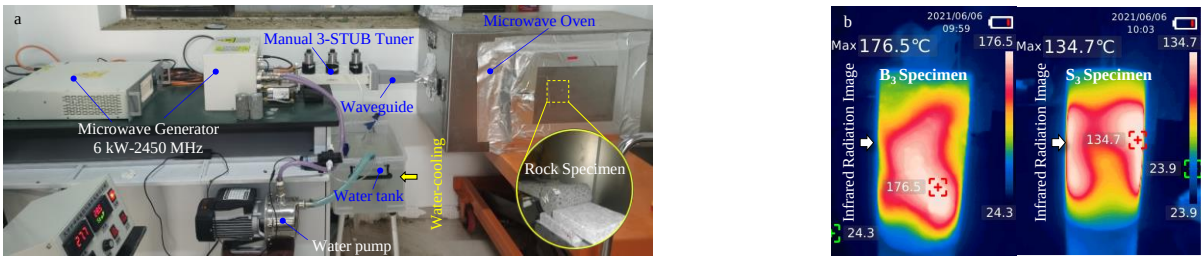

Figure 4. Microwave experimental system and thermal infrared image recording of basalt: (**a**) microwave equipment (2.45 GHz band and 6 kW power) and (**b**) thermal infrared image of basalt after microwave irradiation.

Basaltic rocks, liquid CO_2, and a NaOH or $Ca(OH)_2$ alkaline solution were reacted, and a triaxial mechanical system was used to test the basalt strength at a strain loading rate of 10^{-3}/min. In addition, extensometers were used to monitor the axial and lateral strain of basalt (Figure 5a). In order to simulate the stress conditions suitable for formation pressure, the confining pressure loading was set to 21.0 MPa (Figure 5b). As a result, the stress-strain curve of basalt after CO_2 mineralization was obtained, and the mechanical characteristics and strength differences of basalt before and after microwave irradiation and mineralization were compared. The brittle failure characteristics of the basalt specimens are shown in Figure 5c.

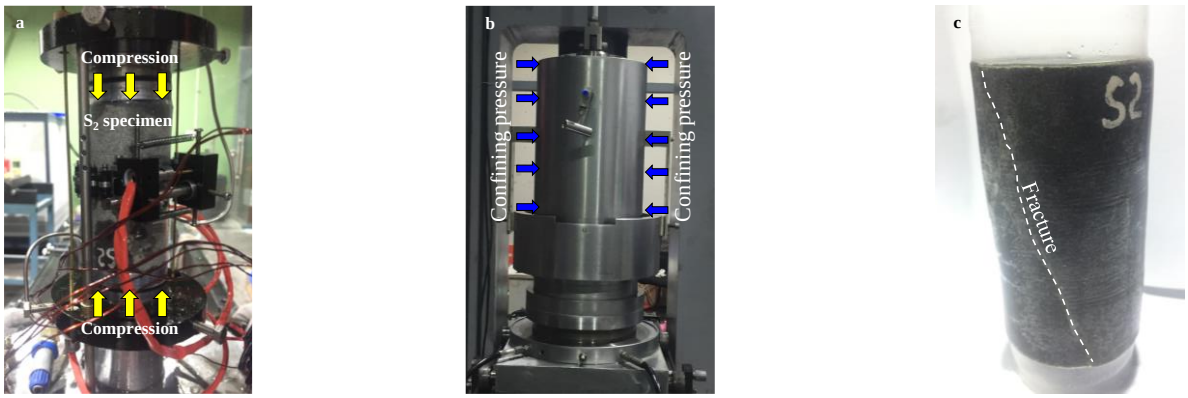

Figure 5. Triaxial mechanical strength test of basalt after CO_2 mineralization: (**a**) specimen setup, (**b**) pressure chamber setup, and (**c**) specimen failures.

2.3. Micro-Structure Analysis of Rocks Using X-ray CT Images

2.3.1. Porosity Calculation Method

The features of the pore structure, fracture structure, and basalt matrix of different basalts were extracted from X-ray CT images using multi-threshold segmentation. Then, a CT three-dimensional reconstruction algorithm was used to reconstruct the volume of the X-ray tomographic image (Figure 6), and the total number of pixels of corresponding pores and fractures in the reconstructed volume image was counted.

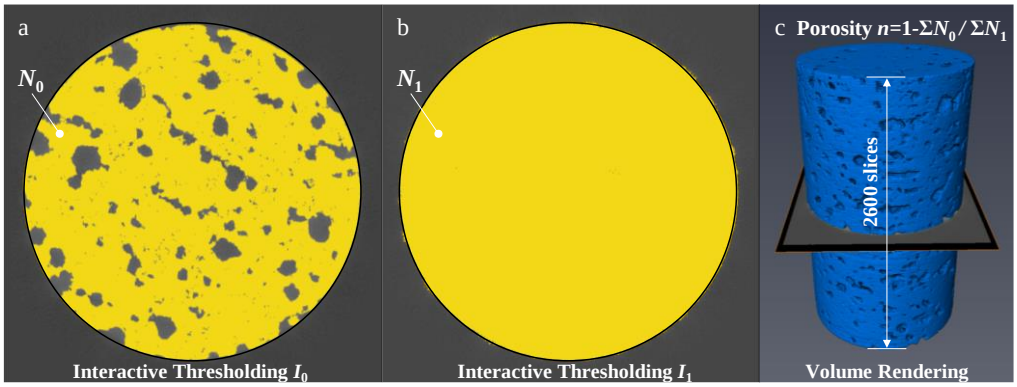

Figure 6. Calculation of basalt porosity by multi-thresholding segmentation and 3D volume reconstruction: (**a**) X-ray image segmentation using interactive thresholding I_0, (**b**) X-ray image segmentation using interactive thresholding I_1, (**c**) 3D volume reconstruction and calculation.

Basalt porosity was calculated using the following formula:

$$n = 1 - \frac{\sum N_0}{\sum N_1} \quad (1)$$

where N_0 is the number of pixels in each slice of the basalt matrix image obtained by multi-threshold segmentation and N_1 is the number of pixels in the whole X-ray CT slice image and the boundary. The error of pixels number is determined by the X-ray images resolution and multi-interactive thresholding.

2.3.2. Permeability Calculation Method

To accurately evaluate the difference in the conductivity of the pores and fractures in basalt to single-phase liquid CO_2 before and after the CO_2 mineralization reaction of basalt, X-ray multi-threshold segmentation and three-dimensional reconstruction methods were used. The change rule of the absolute permeability of basalt was calculated when the pores and fractures in basalt were connected. As it is difficult to accurately identify the

calculation error caused by the air interface when X-ray CT scans the circular boundary of the cylinder sample, the cube model was selected as the scanning range in the cylinder model (Figure 7a) with dimensions of 28 × 28 × 100 mm (Figure 7b).

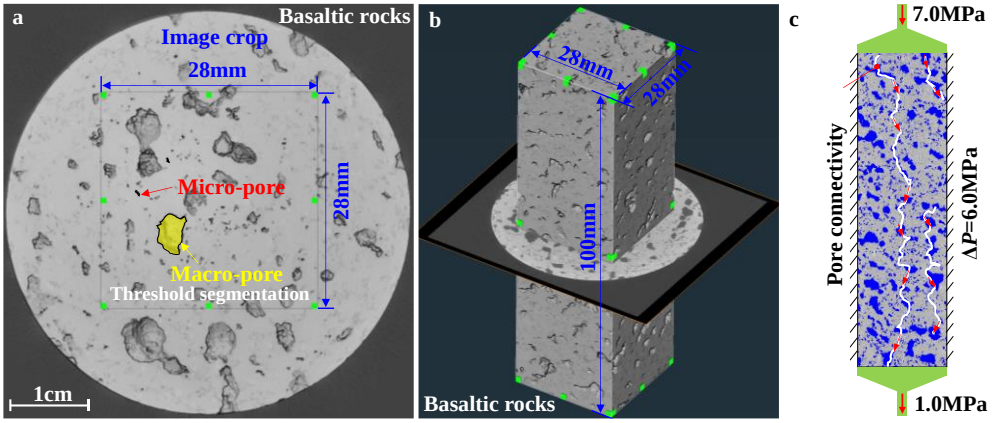

Figure 7. Calculation of basaltic rock permeability using X-ray 3D CT images: (**a**) X-ray image slice, (**b**) 3D volume extraction, (**c**) absolute permeability calculation.

Absolute permeability is defined as the measure of the ability of a porous material to transmit a single-phase fluid, which is an intrinsic property of a material independent of any external condition. Absolute permeability can be derived from Darcy's law as a constant coefficient relating fluid, flow, and geo-material parameters. Therefore, the flow of CO_2 through the pores and fissures in basalt per unit of time was calculated as follows:

$$v_{CO2} = \frac{Q_{CO2}}{S} = -\frac{k}{\mu}\frac{\Delta P}{L} \quad (2)$$

where Q_{CO2} is the global flow rate of liquid CO_2 that goes through the porous medium (unit: m^3/s); S is the cross-section of the sample which the CO_2 fluid goes through (unit: m^2); k is the absolute permeability of basalt reservoir to single-phase liquid CO_2 (cm_2) (unit: m^2); μ is the dynamic viscosity of the flowing fluid (unit: Pa·s); ΔP is the pressure difference applied around the basaltic sample (unit: Pa); L is the length of the sample in the flow direction (unit: m). Q/S is often noted v and accounts for the superficial or mean fluid flow velocity through the porous medium or Darcy's velocity. Only single-phase fluids are considered for absolute permeability. In this study, the absolute permeability can be calculated with X-ray CT images. This experiment simulation module has been developed in AVIZO software (http://www.thermofisher.com/amira-avizo, accessed on 12 October 2022). Liquid CO_2 was used as the lower dynamic viscosity of a single-phase fluid, with a cross-sectional area of S, a length of L, and a pressure difference between the inlet and outlet of liquid CO_2 of ΔP. In order to simulate the matching with the CO_2 injection pressure of the actual formation, the no-flow boundary was set as the condition for absolute permeability calculation with an inlet pressure of 7.0 MPa and an outlet pressure of 1.0 MPa (Figure 7c). In the experiment, the fluid viscosity of single-phase CO_2, defined as μ_{CO_2}, had a value of 1.47×10^{-5} Pa·s.

3. Results and Application

3.1. Enhanced Carbon Mineralization of Basaltic Rocks Induced by Microwave Irradiation

The surface characteristics of basalt samples after mineralization for basalt with two types of pores reacted with liquid CO_2 and a NaOH or $Ca(OH)_2$ solution at a temperature of 30 °C and pressure of 6.0 MPa are shown in Figure 8. The amount of mineralization and scaling on the surface of basalt samples with a large pore structure (B_1, B_2, and B_3) was found to be larger than that of basalt samples with small pores (S_1, S_2, and S_3). In addition, different calcification spots appeared on the surface of each basalt specimen, especially

B_3 and S_3. After microwave irradiation, their mineralization degree was more significant because the microwave thermal effect of basalt was significant. The maximum temperatures of basalt B_3 and S_3 were 176.5 °C and 134.7 °C, respectively. Black hot-melt substances appeared on the surface of basalt B_3 after being irradiated. Microwave irradiation changed the composition of the minerals in basalt. As a result, the strength between the basalt pore channels was reduced. Furthermore, because the high pressure inside the kettle intensifies the carbonization of basalt mineral components, the mineralization reaction and carbon fixation effect of basalt after microwave irradiation were more marked.

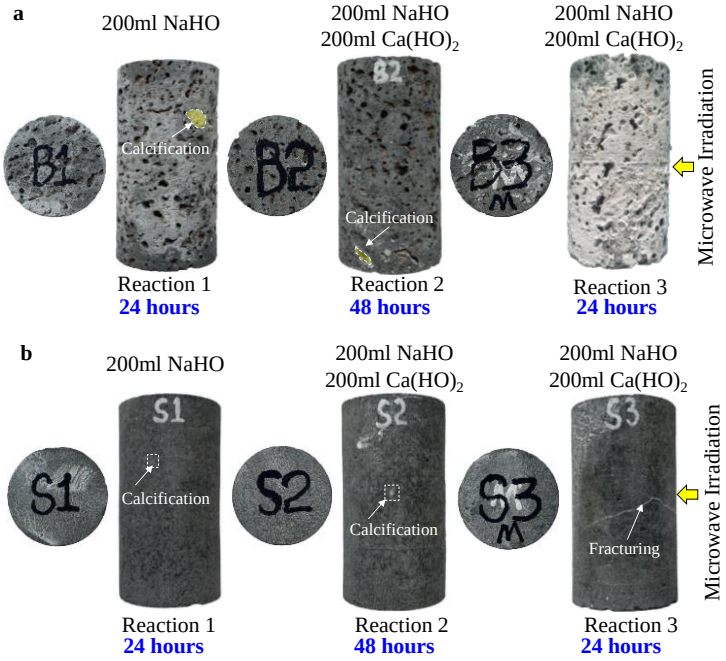

Figure 8. Surface characteristics of the specimen after mineralization and carbon fixation reaction of basalt: (**a**) scaling characteristics on the surface of basaltic rock specimens with macro-porous structure and (**b**) scaling characteristics of basalt surface with a small pore structure.

In order to verify the effect of microwave irradiation on the mineralization and carbon fixation of basalt, X-ray CT scanning was used to reconstruct the internal pore structure of basalt samples after mineralization (Figure 9). The changes in the volume of the connected pores before and after mineralization in the two basalt groups were compared and analyzed (Table 2). The results showed that the CO_2 mineralization reaction of basalt scales block the pore channel, and the volume of connected pores after the mineralization reaction is significantly reduced. In particular, the mineralization reaction of macro-porous basalt was significant, such that the volume of the connected pores in the macro-porous basalt changed markedly before and after mineralization. In addition, basalt mass was calculated before and after the mineralization experimental reaction. Figure 10a shows the comparison of the mass after the mineralization of the two basalt groups. The basalt mineralization reaction in the NaOH and $Ca(OH)_2$ experimental solution group was more marked, while the mineralization and carbon fixation effect of the basaltic rock with a large pore structure was more noticeable. The greatest effect was that of the basalt sample after microwave irradiation, which experienced the largest weight increase after mineralization. Furthermore, the mineralization of basalt via microwave irradiation was found to increase the carbon storage capacity by 2–3 times. Figure 10b shows the changes in the porosity of basalt before and after mineralization according to X-ray CT tomography. As a result, mineralization was found to reduce the porosity of basalt, especially after its mineralization under microwave irradiation. The porosity was reduced at most by approximately 5%. The experimental results are listed in Table 2.

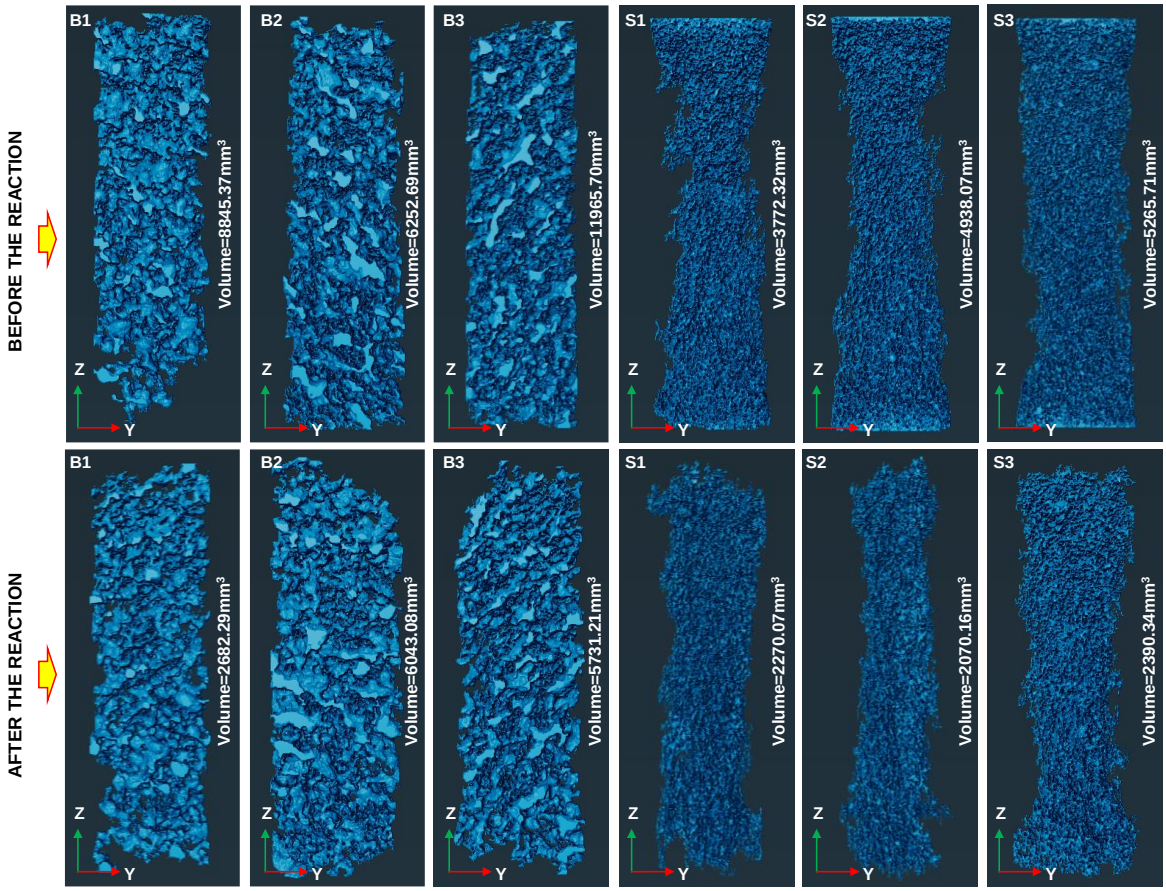

Figure 9. Comparison of pore 3D reconstruction image and connected pore volume.

Table 2. Increase in porosity of basalt before and after mineralization.

Number	Porosity of Basaltic Rocks				Pore Volume of Basaltic Rocks			
	Before the Reaction		After the Reaction		Before the Reaction		Before the Reaction	
	Pore (%)	Effective Porosity (%)	Pore (%)	Effective Porosity (%)	Pore (mm^3)	Connected Pore (mm^3)	Pore (mm^3)	Connected Pore (mm^3)
B_1	14.03	10.63	13.31	3.22	11669.37	8845.37	11070.51	2682.29
B_2	13.86	7.52	12.58	7.27	11527.97	6252.69	10463.34	6043.08
B_3	17.80	14.39	13.07	6.89	14805.04	11965.70	10870.89	5731.21
S_1	5.40	4.54	3.95	2.73	4491.42	3772.32	3285.39	2270.07
S_2	7.32	5.94	3.35	2.49	6088.37	4938.07	2786.34	2070.16
S_3	9.12	6.33	3.95	2.87	7585.51	5265.71	3285.39	2390.34

3.2. Changes in Permeability of Basaltic Rocks Induced by Carbon Mineralization

X-ray CT can be used to acquire and reconstruct the internal structure of basalt before and after mineralization. In this study, Avizo software was used to reconstruct the volume of pores and fractures in basalt in three dimensions. The changes in the absolute permeability before and after the basalt mineralization reaction were evaluated using the absolute permeability experimental simulation function calculation method. Table 3 presents the absolute permeability calculations before and after the basalt mineralization reaction. The simulation results indicate that while the absolute permeability of the two basalts was very different, the absolute permeability of both basalts decreased after mineralization. Among these findings, the absolute permeability of macro-porous basalt was found to decrease more significantly after the mineralization reaction.

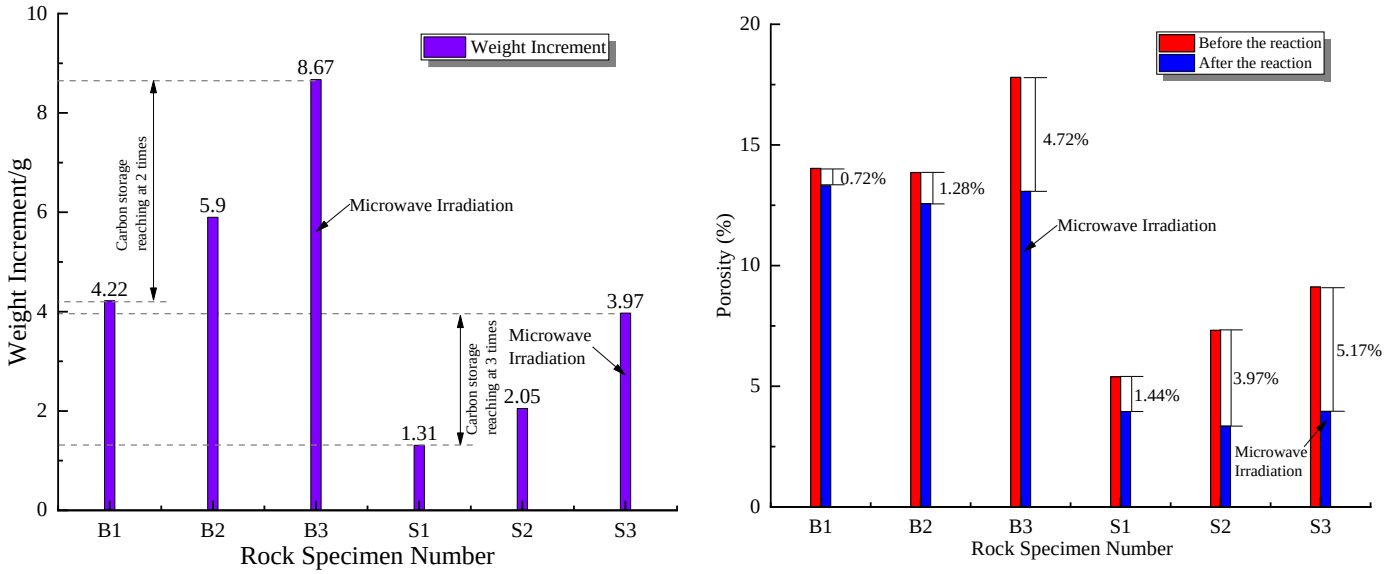

Figure 10. Changes in weight and porosity of basalt after mineralization: (**a**) weight and (**b**) porosity.

Table 4 lists the differences in the absolute permeability of basalt before and after the mineralization reaction. Figure 10 shows the comparison of the absolute permeability values of basalt before and after mineralization. The average absolute permeability of macro-porous basalt before mineralization was 3.90×10^{-12} m^2 (~3.90 Darcy), while the average absolute permeability of macro-porous basalt after mineralization was 0.05×10^{-12} m^2 (~ 0.05 Darcy). Under the same conditions, the average absolute permeability of small-pore basalt before mineralization was 0.02×10^{-12} m^2 (~ 0.02 Darcy), while the average absolute permeability of small-pore basalts after mineralization was 0.007×10^{-12} m^2 (~ 0.007 Darcy). From the three-dimensional reconstructed volume data, it can be observed that the absolute permeability of basalt was related to the connectivity of internal pores and fractures. As shown in Figure 11, the absolute permeability of the macro-porous basalt samples was significantly higher than that of basalts with a small pore structure. The mineralized deposits blocked the internal pore channel of the basalt sample, and microwave irradiation intensified the weakness of the pore structure of the macro-porous basalt. The same reaction pressure broke the pore structure of the basalt. This indicates that the scale formed by the basalt mineralization reaction blocked the pore channel, resulting in a significant decrease in the absolute permeability of the macro-porous basalt after the mineralization reaction. In the CCS project, modifying the pore structure of basalt using microwave irradiation to enhance permeability can be considered a method to improve CO_2 injectability and storage.

3.3. Deterioration in the Strength of Basaltic Rocks Induced by Carbon Mineralization

In this experiment, the pressure condition of the basalts reaction in the autoclave was 6.0 MPa. According to the surface characteristics of basalt after mineralization, only the B_3 and S_3 specimens were found to have local cracks on the surface after being modified by microwave irradiation (Figure 8). However, according to the X-ray three-dimensional fault reconstruction images, no largescale cracks were observed. These results indicate that when the internal pressure of the autoclave is 6.0 MPa, the basaltic sample remains difficult to break. To confirm the weakening of mechanical strength and microwave response of basalt during mineralization, the triaxial rock mechanics test system was used to determine the strength of basalt at the end of the experiment. Lastly, the full stress-strain curve of basalt under the same confining pressure of 21.0 MPa was obtained (Figure 11).

Table 3. Simulation results of absolute permeability of basalt before and after the reaction.

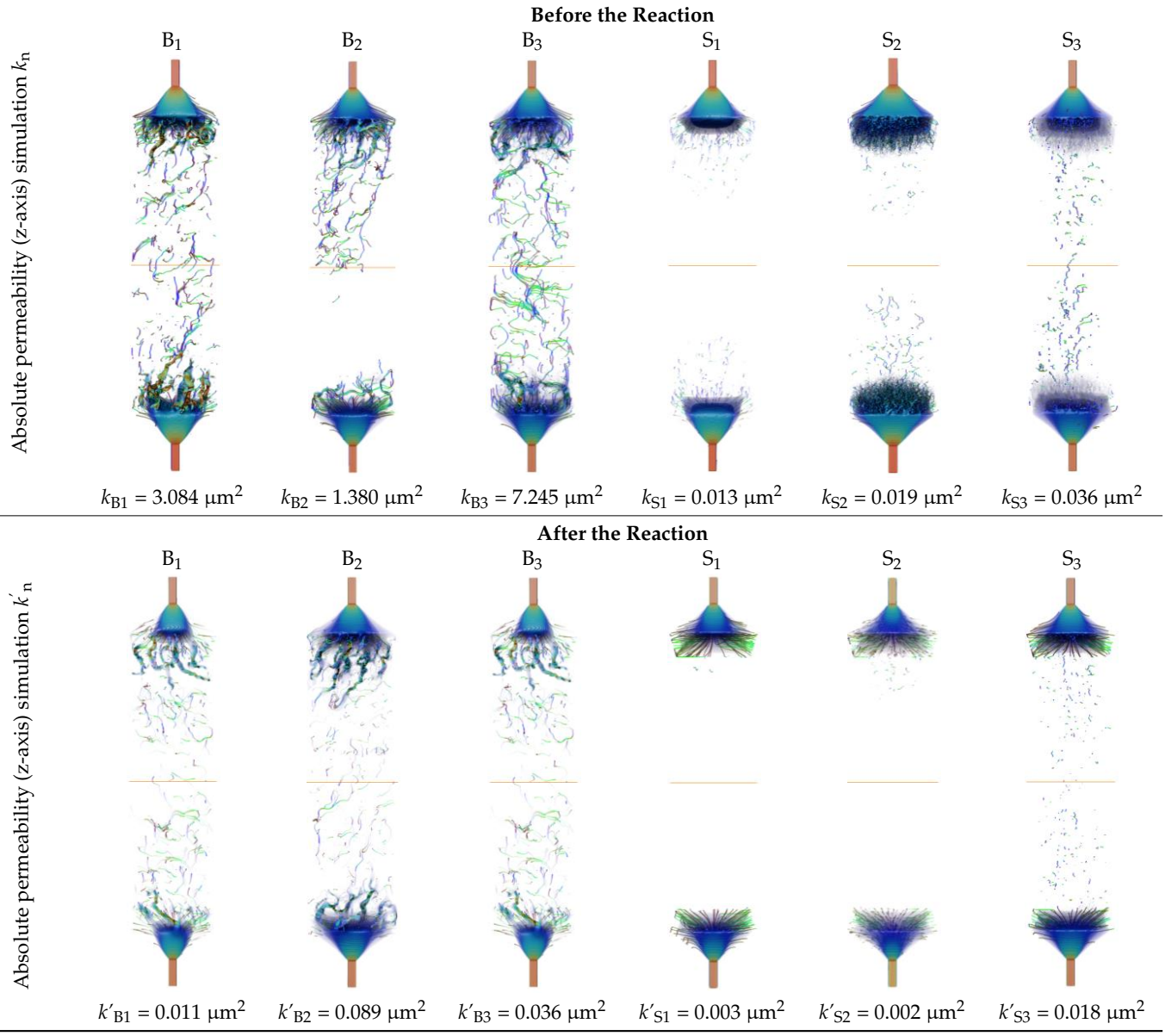

Table 4. Difference analysis of absolute permeability of basalt before and after mineralization reaction.

Name	Absolute Permeability (k/μm²) of Z-axis Direction		Error (%)	Simulation Time	Difference Δk_n/μm²
	Before the Reaction k_n/μm²	After the Reaction k'_n/μm²			
B_1	3.084	0.011	0.003	2.0 days	3.073
B_2	1.380	0.089	0.003	2.0 days	1.291
B_3	7.245	0.036	0.002	2.5 days	7.209
S_1	0.013	0.003	0.002	4.7 days	0.010
S_2	0.019	0.002	0.003	5.2 days	0.017
S_3	0.036	0.018	0.004	5.6 days	0.018

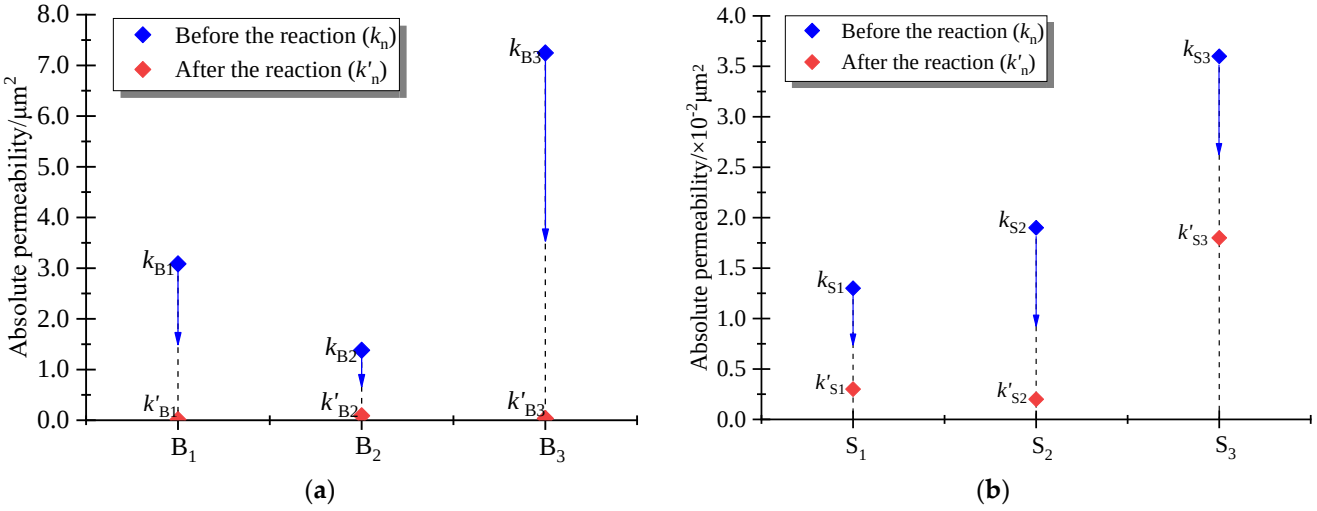

Figure 11. Changes in absolute permeability of basaltic rocks before and after mineralization: (**a**) basalts with macro-porous structure and (**b**) basalts with a small pore structure.

As shown in Figure 12, the two types of basalt showed significant differences in terms of rock strength. Under a confining pressure of 21.0 MPa, the peak strength (σ_c) of small-pore basalts was 584.0 MPa, while the peak strength (σ_c) of macro-porous basalts was only 255.0 MPa. This indicates that the peak strength (σ_c) of macro-porous basalts under the same confining pressure is smaller than the peak strength of small-pore basalts. While the rock strength of the two types of basalts was found to be affected by microwave irradiation, the strength of macro-porous basalts was weakened more significantly under microwave irradiation due to their internal mineral composition. The weakening degree of basalt mechanical strength was analyzed from the reaction of rock CO_2 mineralization. After reacting the basalt B_2 specimen with NaOH and Ca $(OH)_2$ solution under high pressure, it was found that under the confining pressure of 21.0 MPa, the peak strength of the macro-porous basalt B_2 specimen was 141.0 MPa (Figure 11a). Under the same conditions, the weakening effect of the mechanical strength of the small-pore basalt S_2 specimen was not marked, and its strength was still able to reach 572.0 MPa. This is due to the small internal pores, the poor pore connectivity, and the high rock strength. The CO_2 mineralization reaction pressure was not easily transferred to the structural strength of the small pores in basalt. At the same time, there were fewer mineral components in basalt with a small pore structure, and microwave irradiation did not easily change the strength of the basalt mineral matrix. Therefore, the rock strength of small-pore basalt was significantly higher than that of large-pore basalt.

3.4. Enhanced CO_2 Injection in Basaltic Rocks after Microwave Irradiation

In terms of the geological storage of CO_2, basalts with a lower rock strength are better. Furthermore, basalt can achieve a good thermal response under microwave irradiation. As a result, the use of microwave technology has been proposed for rock engineering excavation. With the maturity and commercialization of the CCS project and advances in carbon storage technology, the modification of reservoir pore structures and rock strength using microwave irradiation has been gradually applied to CCUS and CCS projects. In this study, the pore structure, pore connectivity, and rock strength of two types of basalt in the early stage before and after microwave irradiation were evaluated under triaxial conditions. As a result, microwave irradiation was markedly associated with CO_2 mineralization and strength weakening in basalt.

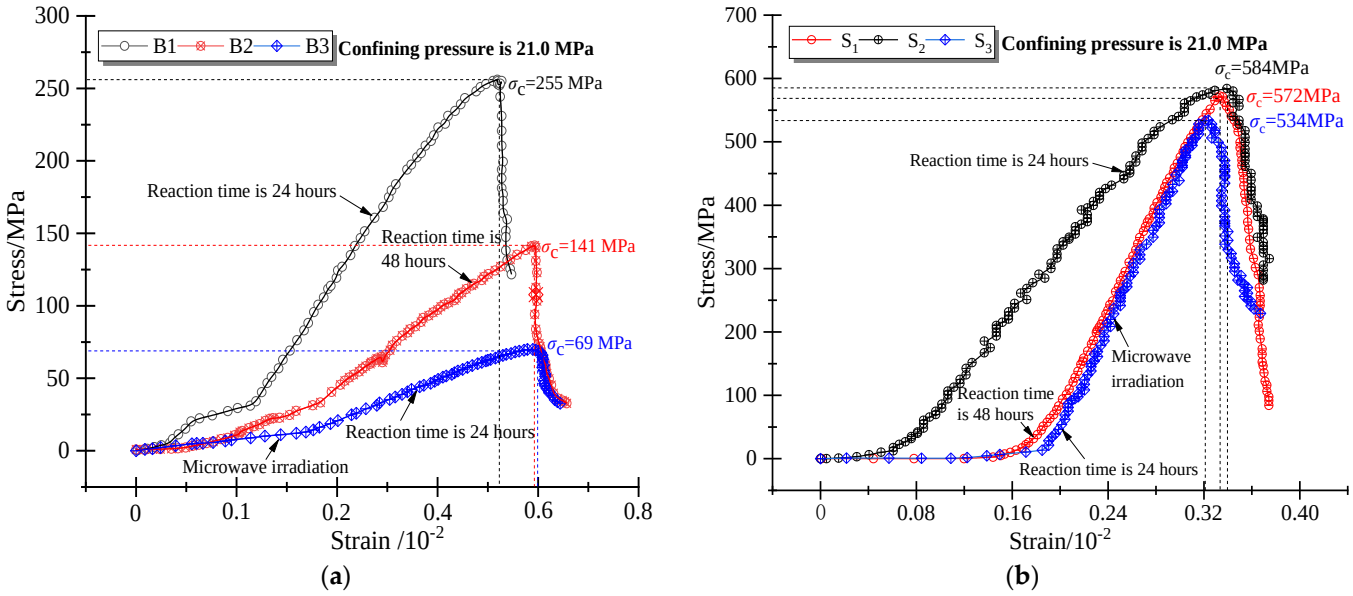

Figure 12. Stress-strain curve relationships of basaltic rocks under confining pressure of 21.0 MPa: (**a**) test results after mineralization reaction of B_1 to B_3 and (**b**) test results after mineralization of S_1 to S_3.

Based on these findings, we propose storage enhancement technology equipment and system design for microwave modification in CO_2 underground storage. The equipment includes a microwave controller, a microwave generator, a reference pin tuner, a water-cooling system, a right-angle waveguide, and a flexible waveguide (Figure 13). Herein, a microwave power supply with a frequency band of 2.45 GHz and a power of 6 kW was selected. The microwave controller controls and shocks the microwave generator. The generated microwave will output a microwave signal through the reference pin tuner and then be led out by the right-angle waveguide and the flexible waveguide. The design of the flexible copper waveguide is shown in Figure 13 I-I, II-II, and III-III. The length of the flexible waveguide is related to the depth of the target layer of carbon sequestration. The flexible waveguide is composed of a corrugated copper tube, which is wrapped with a nitrile rubber to protect the waveguide copper tube. When in use, the flexible copper waveguide should be extended into the drilling. The quartz window of the flexible waveguide should be close to the drilling well wall. The microwave generator generates microwaves and leads them out through the quartz window at the end of the flexible copper waveguide to heat the rocks around the well wall. During this process, as the microwave has attenuation in the copper waveguide, more expensive waveguide materials and manufacturing processes are required to reduce this attenuation. Therefore, microwave irradiation reservoir reconstruction technology is applicable to the target reservoir with a low buried depth (preferably within 150 m), which is the applicable condition of the microwave modification technology proposed in this study.

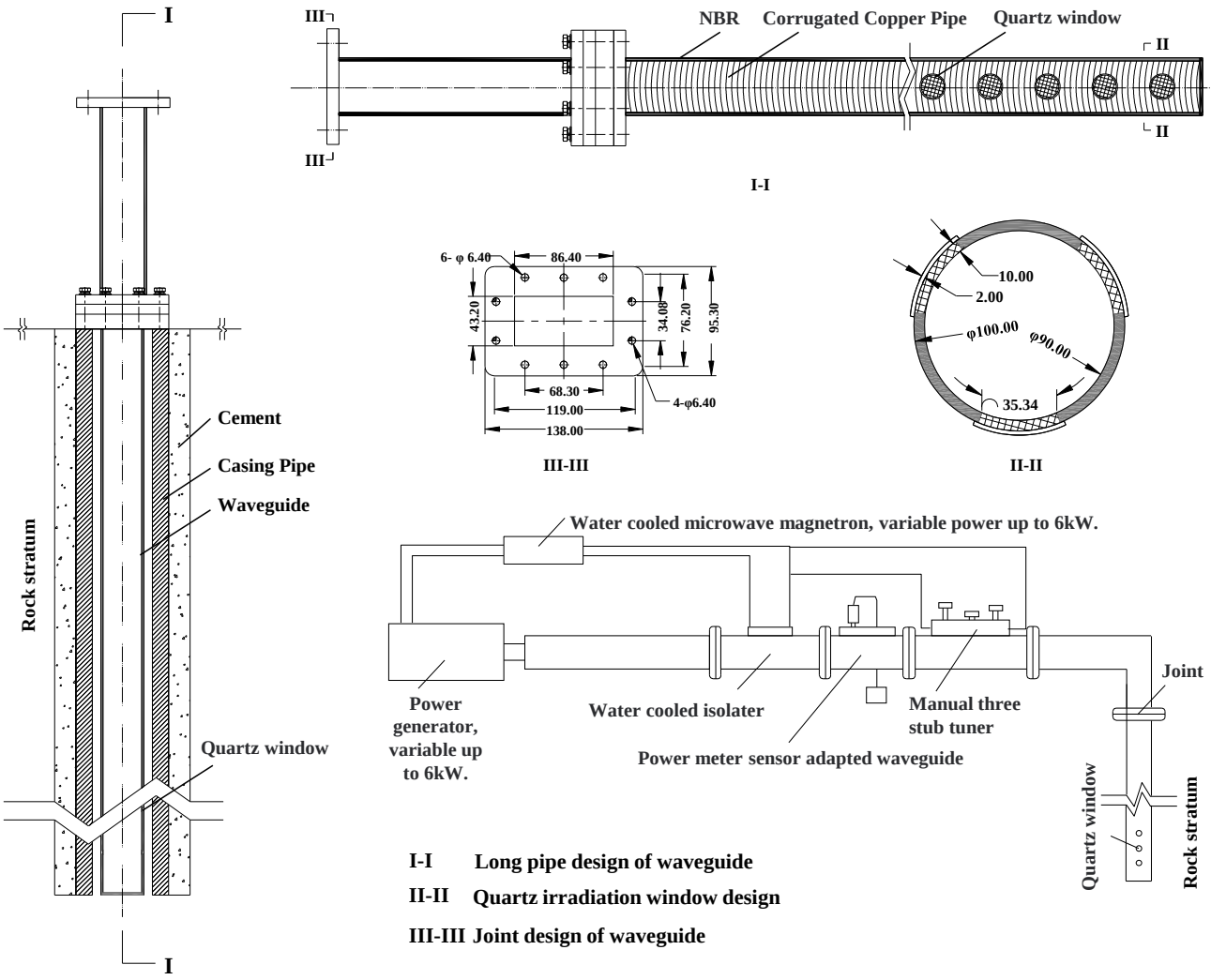

Figure 13. Microwave equipment systems and waveguide design for reservoir rock modification.

4. Discussion

(1) The absolute permeability (k) is computed with a CO_2 single-phase flow. The module takes a feature section using interactive thresholding of labeled images of X-ray CT as input, but each label of the image has to be part either of the solid or of the fluid phase: only one solid and one fluid phase are considered for this calculation. The solid phase is impermeable: there is no flow in it. Therefore, the labeled precise X-ray image is more important for the calculated absolute permeability.

(2) X-ray CT image analysis is applied to the sample from the main basaltic reservoir of the Fushan site in Hainan. Macro-porous basalts obtained a connected porosity and absolute permeability using X-Ray CT images analysis. In this study, the absolute permeability of basalts in the Fushan site was compared with basalts in the CarbFix site using the K–C equation and X-Ray CT images, as listed in Table 5.

(3) The results indicate that microwave modification and storage increase technology are suitable for use in CCS mineralization and storage projects, wherein the basalt well wall can be irradiated with microwaves before the injection well casing is constructed. By using this strategy, it is possible to increase the CO_2 injection rate and reduce the injection well pressure, thereby improving the CO_2 mineralization and both storage efficiency and capacity.

Table 5. The absolute permeability (k) of basalts in the Fushan site compared with the CarbFix site using the K–C equation and X-ray CT images analysis.

K is Calculated Using the K–C Equation (Unit: $\times 10^{-12}$ m^2)			K is Calculated Using X-ray CT Images (Unit: $\times 10^{-12}$ m^2)			
Basalts of the CarbFix site in Iceland [8]	Basalts of the Fushan site in Hainan		Basalts of the CarbFix site in Iceland [8]		Basalts of the Fushan site in Hainan	
K_{Mean}	Macro-porous basalts before the reaction	Small-porous basalts after the reaction	K_V	K_H	Macro-porous basalts before the reaction	Small-porous basalts after the reaction
7.70	49.80 4.92	27.60 0.55	207.00	51.00	3.903 0.022	0.045 0.007

5. Conclusions

In this study, the reaction of basalts with liquid CO_2 and a solution of NaOH and $Ca(OH)_2$ under high pressure was performed, and the mineralization of CO_2 in basalt via microwave irradiation was evaluated. As a result, the changes in the permeability and rock strength of basalts were compared and analyzed. In the following, the main conclusions are summarized:

(1) Both macro- and micro-porous basalts are found within a 50.0 m depth of Fushan Sag in Hainan Province, China. After the mineralization of basalt using liquid CO_2 and a NaOH and $Ca(OH)_2$ alkaline solution under a pressure of 6.0 MPa, this reaction was found to increase the mass and decrease the porosity of both types of basalt. Among the two types of basalt evaluated, the mineralization and carbon fixation effect of macro-porous basalt was found to be more marked. In particular, microwave irradiation was found to increase the carbon storage capacity of basalt by 2–3 times.

(2) After analyzing the X-ray CT images of the basalt samples before and after CO_2 mineralization and comparing the absolute permeability with the plan, we concluded that the absolute permeability of macro-porous basalt was significantly different from that of micro-porous basalt. That is, the absolute permeability of the macro-porous basalt sample was significantly higher than that of the micro-porous basalt sample. Although the mineralized scaling deposits were found to block the pore channels on the surface of the basalt specimens, the high-pressure reaction in the process of basalt mineralization intensified the connectivity of the pore structure. In particular, microwave irradiation reduced the structural strength of the basalt pores. Among the basalt samples, macro-porous basalt was found to experience a significant thermal modification effect upon microwave irradiation, wherein mineralization easily destroyed the pore structure and connectivity. These results indicate that macro-porous basalt had a good degree of permeability and exhibited a marked mineralization effect, making it more suitable for the permanent disposal of CO_2 in CCS projects.

(3) By testing the mechanical strength of basalt before and after CO_2 mineralization, the mechanical strength of macro-porous basalt under a confining pressure of 21.0 MPa was found to be significantly smaller than that of small-pore basalt. While the peak strength of both types of basalts decreased after the mineralization reaction, the weakening effect of high pressure on the rock strength of macro-porous basalt was more significant, and the microwave effect of macro-porous basalt was also highly significant. After microwave irradiation, the mineralization reaction effect of basalt was enhanced, the permeability was also enhanced, and the mechanical strength was weakened, which is conducive to CO_2 storage and injection.

Author Contributions: Z.Y.: Conceptualization, methodology, writing—original draft. H.S. and W.D.: Data curation, software. X.L.: Writing—review and editing. Q.D.: Supervision, writing—review. Q.L.: editing. All authors have read and agreed to the published version of the manuscript.

Funding: Supported by funding support from the National Natural Science Foundation of China (Approval No. 42267021), the National Natural Science Foundation of China (Approval No. 52079068), the National Natural Science Foundation of China (Approval No. 52109120), the Hainan Provin-

cial Science and Technology Foundation of China (Approval No. DYF2022SHFZ106), the Hainan Provincial Natural Science Foundation of China (Approval Nos. 421RC487 and 521QN203), the Open Research Fund Program of the State Key Laboratory of Hydroscience and Engineering (Approval Nos. sklhse-2021-C-02 and sklhse-2021-C-07).

Institutional Review Board Statement: Not applicable.

Informed Consent Statement: Not applicable.

Data Availability Statement: Not applicable.

Conflicts of Interest: The authors declare that they have no known competing financial interest or personal relationships that could have appeared to influence the work reported in this paper.

References

1. Snæbjörnsdóttir, S.Ó.; Oelkers, E.H.; Mesfin, K.; Aradóttir, E.S.; Dideriksen, K.; Gunnarsson, I.; Gunnlaugsson, E.; Matter, J.M.; Stute, M.; Gislason, S.R. The chemistry and saturation states of subsurface fluids during the in situ mineralisation of CO_2 and H2S at the CarbFix site in SW-Iceland. *Int. J. Greenh. Gas Control* **2017**, *58*, 87–102. [CrossRef]
2. Seifritz, W. CO_2 disposal by means of silicates. *Nature* **1990**, *345*, 486. [CrossRef]
3. Mcgrail, B.P.; Schaef, H.T.; Ho, A.M.; Chien, Y.J.; Dooley, J.J.; Davidson, C.L. Potential for carbon dioxide sequestration in flood basalts. *J. Geophys. Res.* **2006**, *111*, B12201. [CrossRef]
4. Alfredsson, H.A.; Oelkers, E.H.; Hardarsson, B.S.; Franzson, H.; Gunnlaugsson, E.; Gislason, S.R. The geology and water chemistry of the Hellisheidi, SW-Iceland carbon storage site. *Int. J. Greenh. Gas Control.* **2013**, *12*, 399–418. [CrossRef]
5. Matter, J.M.; Kelemen, P.B. Permanent storage of carbon dioxide in geological reservoirs by mineral carbonation. *Nat. Geosci.* **2009**, *2*, 837–841. [CrossRef]
6. Kelemen, P.B.; Matter, J. In situ carbonation of peridotite for CO_2 storage. *Proc. Natl. Acad. Sci. USA* **2008**, *105*, 17295–17300. [CrossRef]
7. Park, A.-H.A.; Fan, L.-S. CO_2 mineral sequestration: Physically activated dissolution of serpentine and pH swing process. *Chem. Eng. Sci.* **2004**, *59*, 5241–5247. [CrossRef]
8. Callow, B.; Falcon-Suarez, I.; Ahmed, S.; Matter, J. Assessing the carbon sequestration potential of basalt using X-ray micro-CT and rock mechanics. *Int. J. Greenh. Gas Control* **2018**, *70*, 146–156. [CrossRef]
9. Hövelmann, J.; Austrheim, H.; Jamtveit, B. Microstructure and porosity evolution during experimental carbonation of a natural peridotite. *Chem. Geol.* **2012**, *334*, 254–265. [CrossRef]
10. Ye, Z.N.; Hou, E.K.; Li, H.T.; Duan, Z.H.; Wu, F. Analysis of Gas Content and Permeability Change Pattern of a Coal Reservoir in the Tectonic Positions Based on a THM Coupled Model. *Geofluids* **2021**, *2021*, 5562545. [CrossRef]
11. Aradóttir, E.S.P.; Sonnenthal, E.L.; Björnsson, G.; Jónsson, H. Multidimensional reactive transport modeling of CO_2 mineral sequestration in basalts at the Hellisheidi geothermal field, Iceland. *Int. J. Greenh. Gas Control* **2012**, *9*, 24–40. [CrossRef]
12. Benisch, K.; Bauer, S. Short- and long-term regional pressure build-up during CO_2 injection and its applicability for site monitoring. *Int. J. Greenh. Gas Control.* **2013**, *19*, 220–233. [CrossRef]
13. Grude, S.; Landrø, M.; Dvorkin, J. Pressure effects caused by CO_2 injection in the Tubåen Fm., the Snøhvit field. *Int. J. Greenh. Gas Control.* **2014**, *27*, 178–187. [CrossRef]
14. Ye, Z.; Liu, X.; Dong, Q.; Wang, E.; Sun, H. Hydro-Damage Properties of Red-Bed Mudstone Failures Induced by Nonlinear Seepage and Diffusion Effect. *Water* **2022**, *14*, 351. [CrossRef]
15. Sun, H.; Liu, X.; Ye, Z.; Wang, E. Experimental investigation of the nonlinear evolution from pipe flow to fissure flow during carbonate rock failures. *Bull. Eng. Geol. Environ.* **2021**, *80*, 4459–4470. [CrossRef]
16. Gaus, I. Role and impact of CO_2–rock interactions during CO_2 storage in sedimentary rocks. *Int. J. Greenh. Gas Control.* **2010**, *4*, 73–89. [CrossRef]
17. Li, X.; Li, Q.; Bai, B.; Wei, N.; Yuan, W. The geomechanics of Shenhua carbon dioxide capture and storage (CCS) demonstration project in Ordos Basin, China. *J. Rock Mech. Geotech. Eng.* **2016**, *8*, 948–966. [CrossRef]
18. Major, J.R.; Eichhubl, P.; Dewers, T.A.; Olson, J.E. Effect of CO_2–brine–rock interaction on fracture mechanical properties of CO_2 reservoirs and seals. *Earth Planet. Sci. Lett.* **2018**, *499*, 37–47. [CrossRef]
19. Li, Q.; Lin, B.; Zhai, C. The effect of pulse frequency on the fracture extension during hydraulic fracturing. *J. Nat. Gas Sci. Eng.* **2014**, *21*, 296–303. [CrossRef]
20. Busch, A.; Gensterblum, Y. CBM and CO_2-ECBM related sorption processes in coal: A review. *Int. J. Coal Geol.* **2011**, *87*, 49–71. [CrossRef]
21. Abdulrahman, M.M.; Meribout, M. Antenna array design for enhanced oil recovery under oil reservoir constraints with experimental validation. *Energy* **2014**, *66*, 868–880. [CrossRef]
22. Li, C.F.; Li, Y.; Li, X.M.; Cao, Y.B.; Song, Y.T. The Application of Microbial Enhanced Oil Recovery Technology in Shengli Oilfield. *Pet. Sci. Technol.* **2015**, *33*, 556–560. [CrossRef]
23. Hassani, F.; Nekoovaght, P.M.; Gharib, N. The influence of microwave irradiation on rocks for microwave-assisted underground excavation. *J. Rock Mech. Geotech. Eng.* **2016**, *8*, 1–15. [CrossRef]

24. Feng, X.-T.; Zhang, J.; Yang, C.; Tian, J.; Lin, F.; Li, S.; Su, X. A novel true triaxial test system for microwave-induced fracturing of hard rocks. *J. Rock Mech. Geotech. Eng.* **2021**, *13*, 961–971. [CrossRef]
25. Zheng, Y.L.; Ma, Z.J.; Yang, S.Q.; Zhao, X.B.; He, L.; Li, J.C. A microwave fracturability index (MFI) of hard igneous rocks. *Int. J. Rock Mech. Min. Sci.* **2021**, *138*, 104566. [CrossRef]
26. Lu, G.-M.; Feng, X.-T.; Li, Y.-H.; Hassani, F.; Zhang, X. Experimental Investigation on the Effects of Microwave Treatment on Basalt Heating, Mechanical Strength, and Fragmentation. *Rock Mech. Rock Eng.* **2019**, *52*, 2535–2549. [CrossRef]